Adsorption 10: 29–46, 2004

Measurement and Modeling of Water Vapor Adsorption on Zeolite 4A—Equilibria and Kinetics

A. GORBACH, M. STEGMAIER AND G. EIGENBERGER
Institut für Chemische Verfahrenstechnik, Böblinger Straße 72, 70199 Stuttgart, Germany

Received October 21, 2002; Revised June 16, 2003; Accepted September 5, 2003

Abstract. The adsorption of water vapor on Zeolite 4A has been analyzed. Both equilibrium and kinetics are examined. The equilibrium is measured with a static-volumetric method in a wide range of partial pressure and temperature and is modeled by several conventional approaches and a new type isotherm model, which fitted the obtained data best. Kinetics are determined by measuring breakthrough curves. The breakthrough curves are matched by a detailed model based on a modified linear driving force (LDF) approximation for the mass exchange. An analytic expression for the corresponding LDF-coefficient is designed in order to describe its dependency on water concentration, temperature and pressure. For the practical range of operating conditions the dependency on concentration can be described by the nonlinearity of the adsorption isotherm. The dependency on temperature and pressure corresponds to that of molecular diffusion. The presented data and models for equilibria and kinetics provide a basis for modeling and optimizing air-drying processes containing Zeolite 4A.

Keywords: adsorption, zeolites, water vapor, equilibria, kinetics, modeling

1. Introduction

Since the invention of the "heatless dryer" (Skarstrom, 1972), there has been significant progress in the design and modeling of air drying processes based on pressure swing adsorption (PSA). Particulary in small scale applications such as the drying of instrument air, PSA processes are widely used and have become the method of choice (Ruthven, 1984). Essentially dry air can be readily obtained with either alumina or zeolite (4A or 5A) as the dessicant, but beaded alumina is usually selected. Since the equilibrium isotherm for water vapor on alumina is less nonlinear, i.e. less strongly curved than the corresponding isotherm for zeolite, the effective working capacity in a PSA system is higher. Moreover alumina beads show less attrition under the rough operating conditions. However, to obtain bone dry air (1 ppm H_2O or less), layered beds should be used, combining the high working capacity of alumina or other gels with the strong hydrophilicity of zeolites.

Due to the high complexity of the system dynamics, a priori simulations with detailed computer based models are more and more used for PSA unit design. Usual design considerations are high productivity and recovery as well as product purity. To ensure the desired operating conditions, it is crucial that the model used matches both equilibria and kinetics sufficiently well. Concerning product purity, it is of high importance to fit the very low concentration range at the end of the bed. In a layered design this is determined by the strong nonlinearity of the adsorption equilibrium of the water-zeolite system and its kinetics. Although water adsorption isotherms have been measured at high to moderate vapor concentrations, there has been little work to explore the equilibrium and kinetic data at very low concentrations and loadings. In addition, the few studies available revealed significant differences in the measured data.

In this paper we shall present measurements and corresponding models of both equilibria and kinetics of water vapor adsorption on Zeolite 4A as a

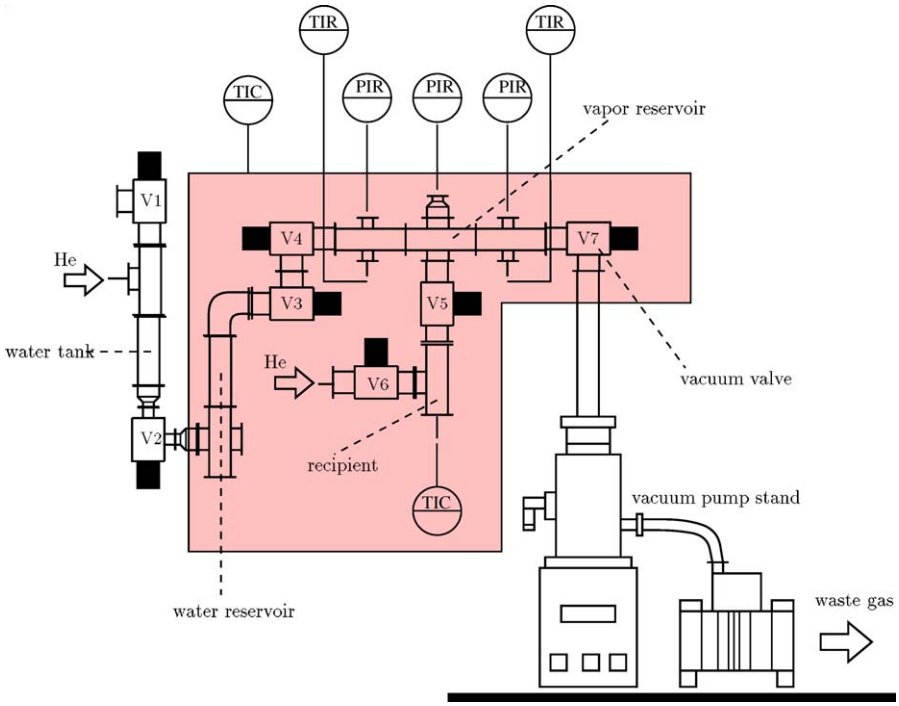

Figure 1. Simplified process flow sheet of the automated isothermal equilibrium apparatus.

function of temperature over a wide range of water vapor concentration.

2. Experimental Setup

2.1. Equilibrium Apparatus

For measuring the thermodynamic equilibrium between water vapor in the gas phase and water amount adsorbed on the zeolite, an automated equilibrium apparatus was developed. Figure 1 gives a simplified process flow sheet. The principle of operation is static-volumetric.

In order to obtain data over a wide range of partial pressure down to the significant range of the isotherm nonlinearity, it is indispensable to evacuate the system to high vacuum by a sequence of a membrane and a turbo-molecular pump. The set-up is mainly built of standard vacuum parts ensuring infinitesimal small leakage ($<10^{-9}$ mbar l/s). The rigorous requirements concerning the sensors are fullfilled by using calibrated resistance temperature sensors (Pt100, tolerance class A) as well as three temperature controlledqry capacitive pressure gauges (MKS Baratron, type 127A: $10^{-4}-1$ mbar, type 128A: $10^{-2}-100$ mbar, type 122A: $10^{-1}-1000$ mbar —0.15% accuracy of reading). Signals are conditioned with 22 bit resolution (HP 34970A multiplexer). To maintain constant temperature within the whole system, all parts are embedded in a thermostat system, as can be seen in Fig. 2. The free space between vacuum parts and the surrounding jackets is filled with small aluminum pellets. Due to the large time constant for attaining equilibrium and the required amount of measurements, the entire measurement system is fully automated. The LabVIEW programming language is used to both control and monitor the system.

After a specific temperature is set, the zeolite is activated in situ. Therefore the sampling device can be heated to high temperature ($>500°$C) while being purged with helium under vacuum condition. The system is then evacuated to high vacuum before a specific amount of water from the water reservoir is evaporated into the vapor reservoir. The adsorptive is gas free permeate from reverse osmosis stored in a water tank under helium atmosphere (Fig. 1). Knowing the exact volumes,[1] temperature and an appropriate equation of state,[2] the pressure difference before and after opening the valve to the recipient

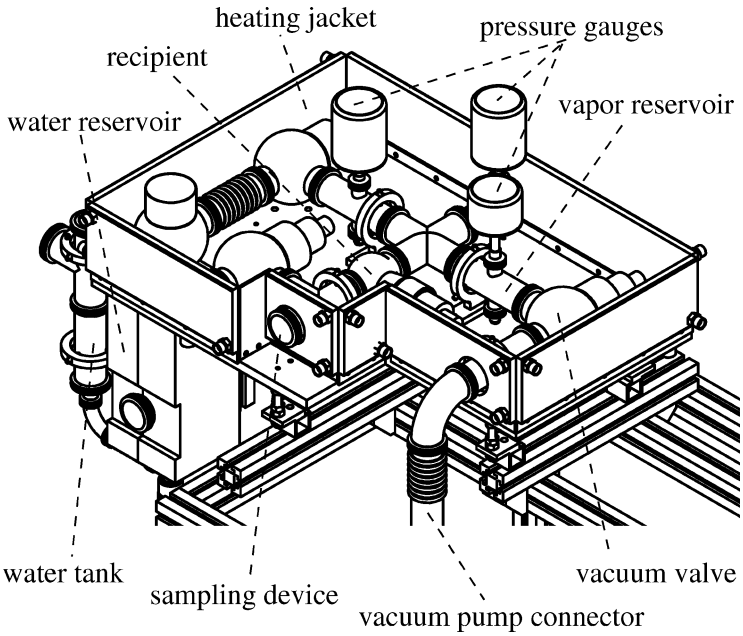

Figure 2. Sketch of the thermostated section of the equilibrium apparatus.

with the sample, can be used to calculate the amount adsorbed.

Under these conditions, the most important source of errors is related to the adsorption of water vapor on the inner surface of the stainless steel apparatus. In order to quantify this effect the loading is measured without any adsorbent being in the sampling device. Figure 3 shows the result at 25°C. It can be seen that the absolute value of the measured loading is less than 1% of the later measured actual loading of the zeolite at the corresponding partial pressure. In the region of feasible operating conditions this error is even below 1‰. Hence, we can conclude, that in the parameter region of interest the error caused by adsorption on the metal surface is negligible.

2.2. *Kinetic Apparatus*

In order to determine coefficients for heat- and mass-transfer, a common dynamic-column breakthrough approach is used (e.g. Malek and Farooq, 1997). Figure 4 depicts the process flow sheet of the experimental setup. There are four subsystems that comprise the main apparatus. (1) The water delivery system: to generate a feed stream with defined moisture content, a controled hydrogen flow is mixed with a controled flow of synthetic air and then oxidized in a catalytic reactor before it is cooled down to the desired temperature. Since hydrogen reacts completely the error of the moisture content is in the range of the inaccuracy of the mass flow controllers (<1%). (2) The adsorber: the adsorbent pellets are filled in a stainless steel tube, 80 cm in length, 10 mm inner diameter. The heating of the jacket allows to control the wall temperature and is used for in situ desorption, supported by a helium purge and a vacuum pump (190°C, 1 mbar). The system pressure is set and held constant by a control valve (MKS, type 248A) at the adsorber outlet. Two thermocouples (NiCrNi type K, 0.5 mm), one at the inlet and one at the outlet, register changes in temperature. (3) Water vapor concentration is measured with a mass spectrometer (Balzers ThermoStar) which allows to monitor fast changes in moisture over a wide range with high resolution. (4) Data acquisition and process control: as before, full automation and monitoring of the system is achieved with LabVIEW.

After the adsorbent is activated, the adsorber and the bypass are evacuated below 1 mbar. Thereafter, the adsorber is purged with carrier gas (synthetic air) while being tempered to the desired adsorption temperature. The desired adsorption pressure is set and maintained by a pressure controller (MKS, type 250). Now, the adsorber is closed at both ends and moist feed air flows

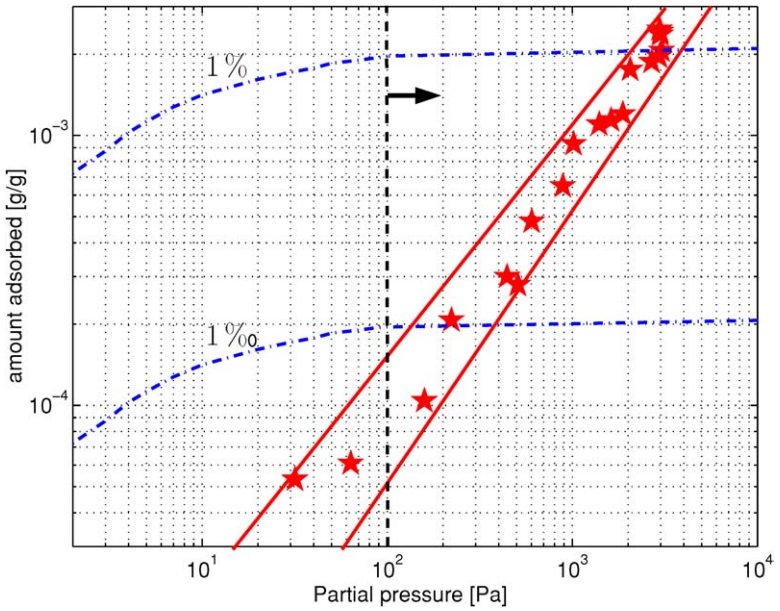

Figure 3. Zero loading test at 25°C: Symbols denote measurements defining the actual error region (surrounded by solid lines); The dot-dashed lines mark the amount of 1% (top) of the later measured defacto loading and 1‰ (bottom) respectively; Right from the dashed line is the region in which the zeolite is saturated with water.

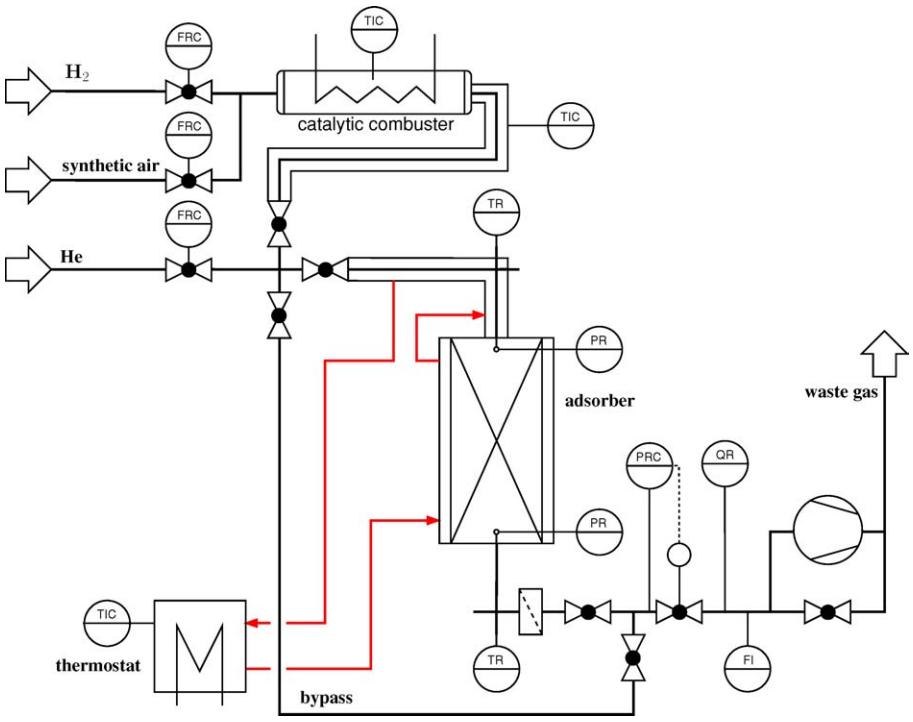

Figure 4. Simplified process flow sheet of the breakthrough experiments.

through the bypass until the concentration of the feed gas, set by the two mass flow controllers, is adjusted and the feed pressure is set to adsorption pressure. The measurement starts when the adsorber valves open and the bypass valves close simultaneously.

3. Results and Discussion

3.1. Equilibrium Data and Modeling

3.1.1. Measurements. Figure 5 shows the measured equilibrium data of water vapor adsorption on a commercial Zeolite 4A provided by Grace Davison Chemicals (1 mm cylindrical pellets) at four temperatures over a range of six decades of partial pressure.

The results displayed in linear scale (Fig. 5, top) show that the isotherm is highly nonlinear and its slope and the absolute loading change with temperature as expected. One may conclude that the shape of the isotherm is of type I (Brunauer et al., 1940). Indeed, parameter fits to models of type I (Münstermann et al., 1983) are reported. In order to analyze the equilibrium at lower pressures, a logarithmic plot gives a deeper insight (Fig. 5, bottom). In this plot the isotherm shows two turning points and thus resembles more a type IV isotherm.

As an aside, it is worth pointing out that this behavior is not unexpected if we take calorimetric measurements into account. Precise values of the enthalpy of adsorption as a function of loading have been tabulated by Zhdanov et al. (1981). One important result is that there is a region of very high enthalpies (100 kJ/mol) for very small loadings, followed by a steep decrease down to an almost constant value (below 60 kJ/mol). This can be described by the following adsorption mechanism: Assuming a completly dehydrated zeolite, the first water molecules adsorbing interact with the relatively weakly bonded Na^+ cations. These interactions are very strong and hence the heat of adsorption is high where the coverage is small (up to 3 moles of water per zeolite unit cell). As adsorption develops, the process is governed by the interaction of adsorbate molecules with specific adsorption centers that are not mobile, introducing a region of lower adsorption enthalpies. Thus we can conclude that the two plateaus in calorimetric measurements, representing two different adsorption sites, correlate with the two plateaus observed in the equilibrium data shown in Fig. 5.

This behavior requires in situ desorption, in order to guarantee reproducible initial conditions. Zhdanov showed that the evacuation of Na-A zeolite at room temperature leads to the removal of twenty of the twenty six water molecules contained in the unit cell of hydrated zeolite. The remaining six are only desorbed at temperatures above 150°C.

3.1.2. Modeling. In order to successfully model air drying processes it is crucial to fit the equilibrium data to an analytic expression, i.e. a proper adsorption isotherm model. The program package ADSEQ, an object-oriented toolbox developed at our Institut, was used to store both experimental data and conventional or user supplied isotherm models in a database. Since the toolbox is implemented in MATLAB, its non-linear least squares optimizer is used to determine model parameters.

Figure 6 shows the result of a parameter fit for eighteen commonly used isotherm models. The corresponding model equations and nomenclature are listed in Table 1. The graph displays the logarithm of the relative standard deviation (STD) between model fit and experimental data, i.e. the capability of the isotherm equation to model the data in the whole region of temperature and partial pressure. As a first result we can conclude that none of the applied models fit the data appropriately. The lowest STD obtained is about 7% (model no. 7). However, it is important to underline that this model (a combined Freundlich-Dubinin-Astakhov approach) has to be fitted to every temperature separately, i.e. the parameters do not depend on temperature. Using one parameter set for all temperatures with only the relative humidity Φ depending on temperature, leads to STDs far beyond those shown in Fig. 6. The best result with parameters with a specific temperature dependency is obtained with model no. 15 (Sips3T0). Figure 7 displays the equilibrium data and the model fit in logarithmic scale as well as the deviation. For larger values of partial pressure, the model fits the data quite well. However, for very small partial pressures, the small absolute deviation results in a large relative STD of about 40%. This result emphasizes the relevance of both, enough data in the area of very low concentration and its representation in a log-scale to evaluate model deviations properly.

Since conventional adsorption isotherm models proved to be not applicable, a new isotherm model has been considered. It has to display two turning points (as seen in Fig. 5, bottom), a Henry region for very low

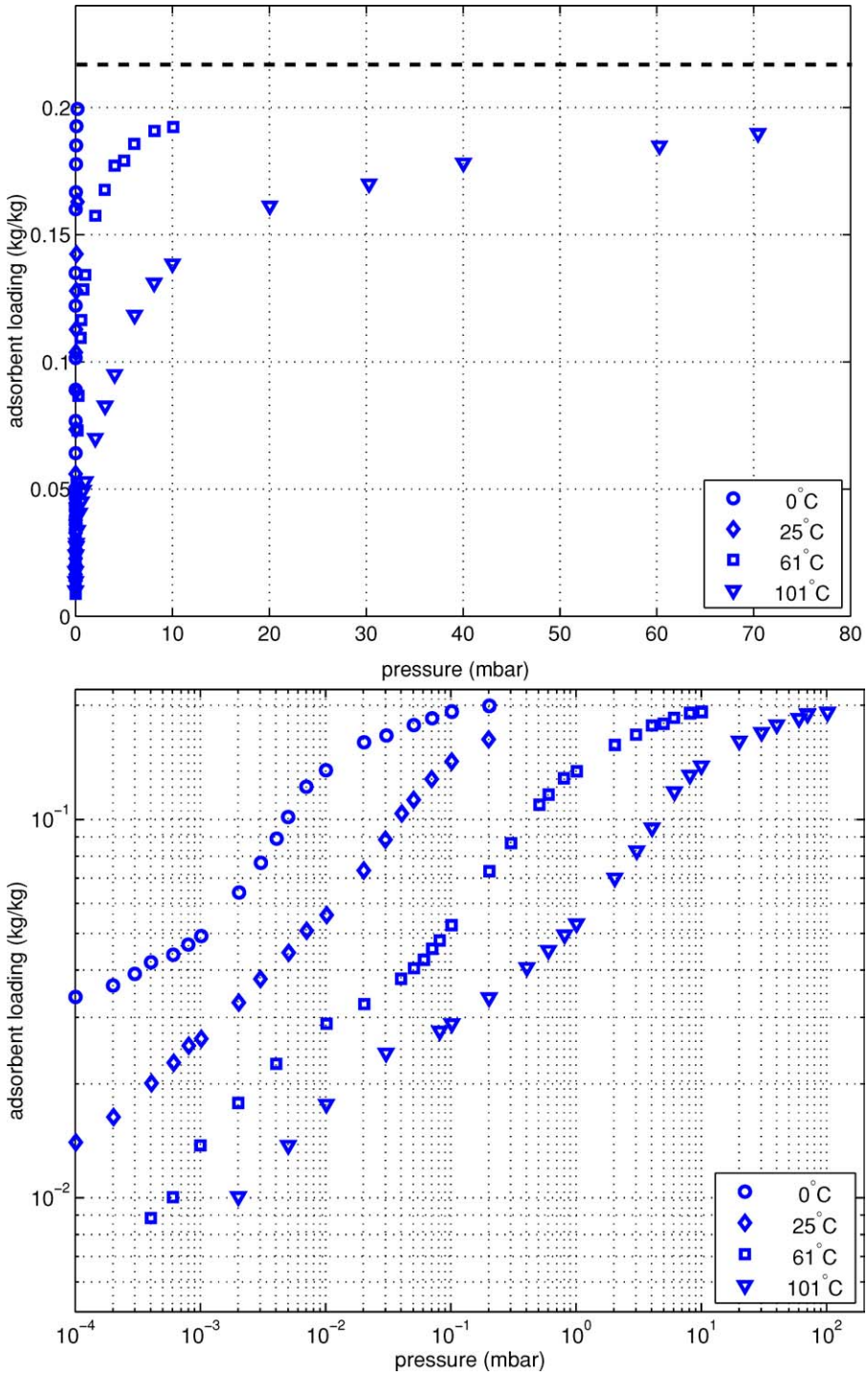

Figure 5. Equilibrium data of water vapor on Zeolite 4A at four different temperatures: linear (top) and logarithmic scale (bottom). The dashed line indicates the maximum loading reported in literature (Zhdanov et al., 1981).

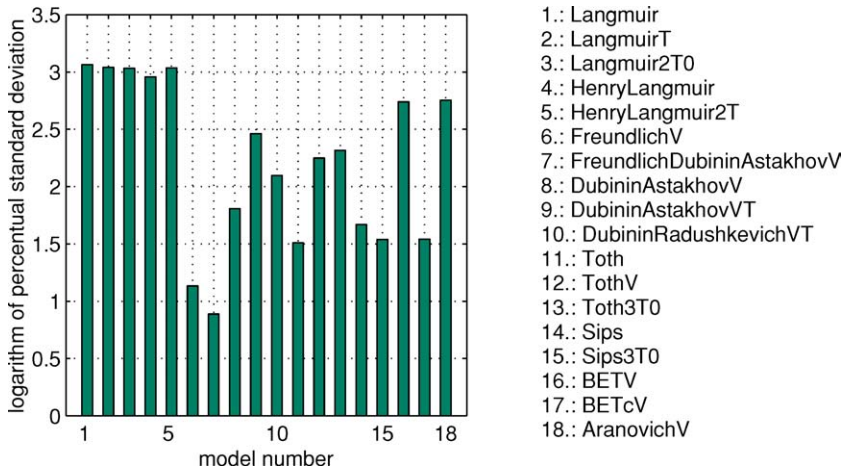

Figure 6. Logarithm of relative standard deviation of several isotherm models specified in Table 1 after a least squares fit to the measured data.

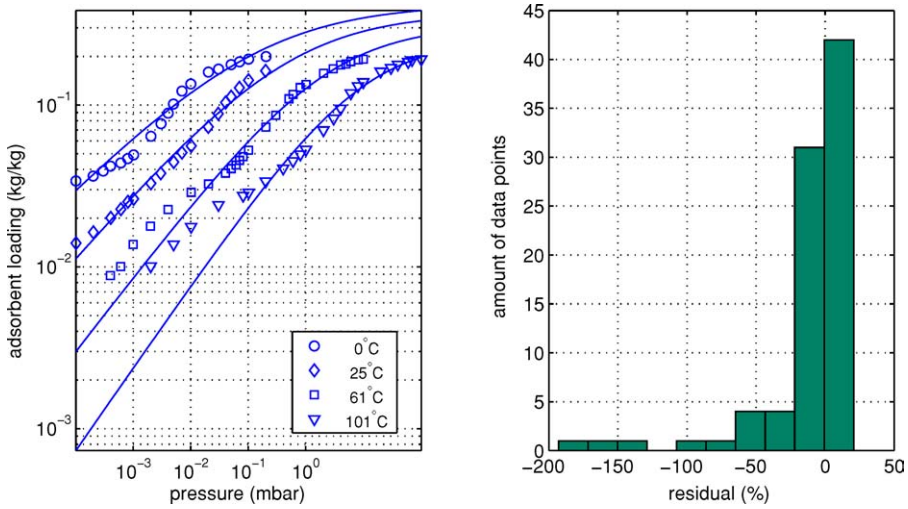

Figure 7. Left: Equilibrium data (symbols) and model fit with a Sips approach (model no. 15) at different temperatures. Right: Relative deviation between experimental data and model.

partial pressures, and a region of saturation for high humidities to maintain physical consistency. A simple function that fulfills these requirements is a rational class model with both 2nd order denominator and numerator as shown in Eq. (1).

$$X(b_{0..4}, p_j) = b_0(T) \cdot \frac{b_1(T) \cdot p_j + b_2(T) \cdot p_j^2}{1 + b_3(T) \cdot p_j + b_4(T) \cdot p_j^2} \tag{1}$$

The loading X depends on the partial pressure of water p_j as the independent variable as well as on five temperature dependent parameters $b_{0..4}$. The temperature dependence of the parameters is assumed to follow van't Hoff's law:

$$b_0(T) = b_{0,0} \cdot e^{b_{0,T} \cdot (1 - T/T_0)} \tag{2}$$

$$b_{1..4}(T) = b_{1..4,0} \cdot e^{b_{1..4,T} \cdot (T_0/T - 1)} \tag{3}$$

For the sake of a well conditioned nonlinear least squares regression problem the temperature is scaled with the reference temperature T_0. Figure 8 shows the result for the least squares fit of the above model to the measured data. It can be seen that both in linear and log-scale the model fits the data well over the whole

Table 1. Names and equations of applied conventional adsorption isotherm models (Fig. 6).

No.	Model name	Equation	Parameters
1	Langmuir	$q = q_s \frac{bp}{1+bp}$	2
2	LangmuirT	$q = q_s \frac{b(T)p}{1+b(T)p}$ $b(T) = b_\infty \exp(b_T/T)$	3
3	Langmuir2T0	$q = q_s(T) \frac{b(T)p}{1+b(T)p}$ $b(T) = b_0 \exp(b_T(T_0/T-1))$ $q_s(T) = q_{s0} \exp(q_{sT}(1-T/T_0))$	4
4	HenryLangmuir	$q = Kp + q_s \frac{bp}{1+bp}$	3
5	HenryLangmuir2T	$q = K(T)p + q_s \frac{b(T)p}{1+b(T)p}$ $b(T) = b_\infty \exp(b_T/T)$ $K(T) = K_\infty \exp(K_T/T)$	5
6	FreundlichV	$q = K\Phi^n$	2
7	FreundlichDubininAstakhovV	$q = K\Phi^m + q_s \exp(-(a\log(1/\Phi))^n)$	5
8	DubininAstakhovV	$q = q_s \exp(-(a\log(1/\Phi))^n)$	3
9	DubininAstakhovVT	$q = q_s \exp(-(aT\log(1/\Phi))^n)$	3
10	DubininRadushkevichVT	$q = q_s \exp(-(aT\log(1/\Phi))^2)$	2
11	Toth	$q = q_s \frac{bp}{(1+bp^t)^{1/t}}$	3
12	TothV	$q = q_s \frac{b\Phi}{(1+b\Phi^t)^{1/t}}$	3
13	Toth3T0	$q = q_s(T) \frac{b(T)p}{(1+b(T)p^{t(T)})^{1/t(T)}}$ $b(T) = b_0 \exp(b_T(T_0/T-1))$ $q_s(T) = q_{s0} \exp(q_{sT}(1-T/T_0))$ $t = t_0 + t_T(1-T_0/T)$	6
14	Sips	$q = q_s \frac{(bp)^n}{(1+(bp)^n)}$	3
15	Sips3T0	$q = q_s(T) \frac{(b(T)p)^n(T)}{(1+(b(T)p)^n(T))}$ $b(T) = b_0 \exp(b_T(T_0/T-1))$ $q_s(T) = q_{s0} \exp(q_{sT}(1-T/T_0))$ $n = n_0 + n_T(1-T_0/T)$	6
16	BETV	$q = q_s c \frac{\Phi}{(1-\Phi)(1+(c-1)\Phi)}$	2
17	BETcV	$q = q_s\left(\frac{\Phi}{1-\Phi} + \frac{\alpha}{2\beta}\right)$ $\alpha = 2\Phi(b-1) + 2\Phi^2(b-1)^2 + \Phi^n(Nb^2+Nh-N^2b^2) + \Phi^{N+1}(2b+N^2b^2+2Nb-2b^2 - Nb^2-2h-2Nh) + \Phi^{N+2}(Nh+2h)$ $\beta = 1 + 2\Phi(b-1) + \Phi^2(b-1)^2 + \Phi^N(b^2+h-2b+Nb^2) + h\Phi^{N+2} + \Phi^{N+1}(Nb^2+2b-2b^2-2h)$	4
18	AranovichV	$q = q_s c \frac{\Phi}{(1-\Phi)^{0.5}(1+c\Phi)}$	2

region of partial pressure and for all temperatures. The corresponding parameter values are listed in Table 2. A plot of the relative error (Fig. 9) shows the deviation ratio for all data, i.e. the fraction of model predicted loading and actually measured loading. With a STD of approximately 5% (Sips3T0: 40%) and a maximum relative deviation of 12.5% (Sips3T0: 180%) this result is quite acceptable.

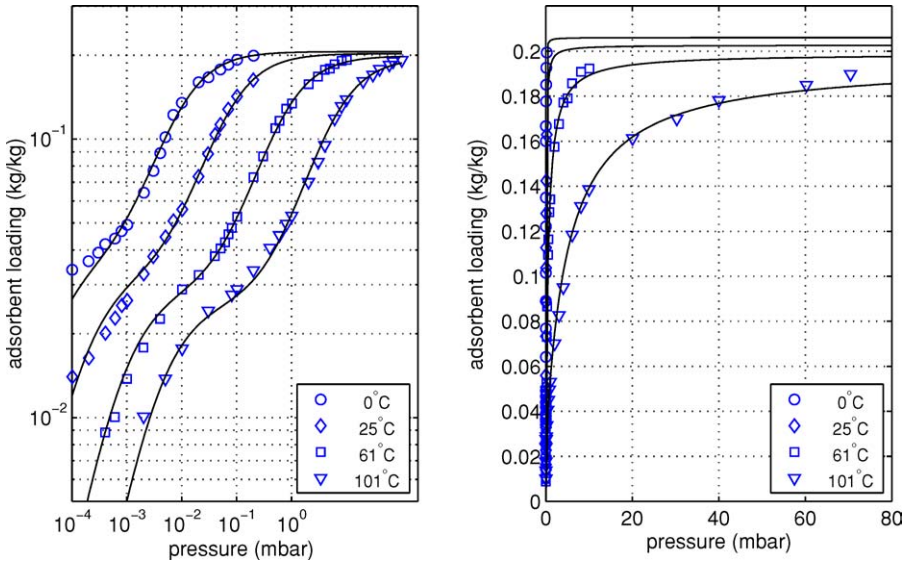

Figure 8. Equilibrium data (symbols) and model fit with the new approach (Eq. (1)) at different temperatures in linear (right) and logarithmic scale (left).

Table 2. Parameter values and units for the new type isotherm model (Eq. (1)) after a least squares fit to the measured equilibrium data (Fig. 5).

Parameter	Value	Unit
$b_{0,0}$	$1.18003 \cdot 10^{-2}$	kg/kg
$b_{1,0}$	$2.03629 \cdot 10^{-3}$	mbar^{-1}
$b_{2,0}$	$1.75732 \cdot 10^{-10}$	mbar^{-2}
$b_{3,0}$	$2.24522 \cdot 10^{-3}$	mbar^{-1}
$b_{4,0}$	$1.22430 \cdot 10^{-11}$	mbar^{-2}
$b_{0,T}$	$5.0 \cdot 10^{-6}$	–
$b_{1,T}$	18.4468	–
$b_{2,T}$	41.3509	–
$b_{3,T}$	17.2808	–
$b_{4,T}$	41.1549	–
T_0	273.25	K

Figure 10 shows a comparison between a model fit with the new approach Eq. (1) based on our measurements and the equilibrium isotherms for the Linde-A Zeolite-Water Vapor System published by Union Carbide (Morris, 1968; Breck et al., 1956). The Carbide data has been widely used by researchers and design engineers.

In the following, the equilibrium will be described by the molar loading q instead of X where $q(p_j, T) = X(p_j, T)/M_{\text{H}_2\text{O}}$.

3.2. Kinetic Data and Modeling

3.2.1. Measurements. Breakthrough experiments were carried out for three different temperatures and two different bed pressures. The experimental apparatus, procedure and analysis have been discussed earlier. Table 3 provides some relevant data on the adsorbent used as well as other information regarding the experiments (case A–D) which are needed for the following modeling.

Figure 11 shows a typical result of the signals measured at the adsorber outlets (see Fig. 4), i.e. the temperature and the molar fraction of water. It should be noted here that the measured molar fraction before breakthrough is not equal to zero due to a zero shift in the mass spectrometer signal. As can be seen, the breakthrough occurs only after 23.5 h. This is due to the very low water concentration and the high capacity of the Zeolite. As a consequence, any flow nonidealities at the adsorber inlet can be neglected. The shape of the concentration breakthrough curve seems almost point-symmetric to the center of the front. This result is not expected if one considers the high nonlinearity of the adsorption isotherm. However, since the shape is also influenced by the adsorption kinetics as well as the coupling of heat- and mass-transfer, it is crucial to analyze these phenomena thoroughly in order to understand the system response and to model the column dynamics properly.

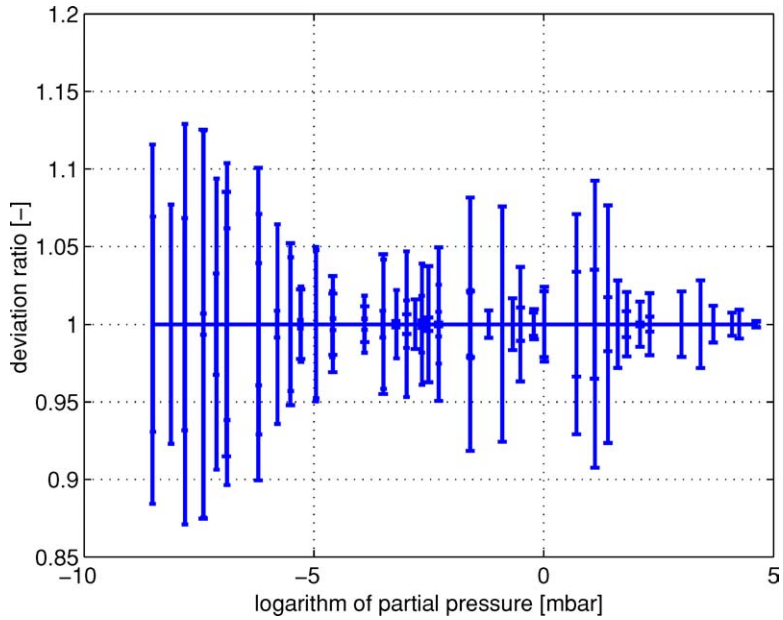

Figure 9. Maximum error range: ratio between experimental data and new type model (Eq. (1)) for all measured temperatures and partial pressures.

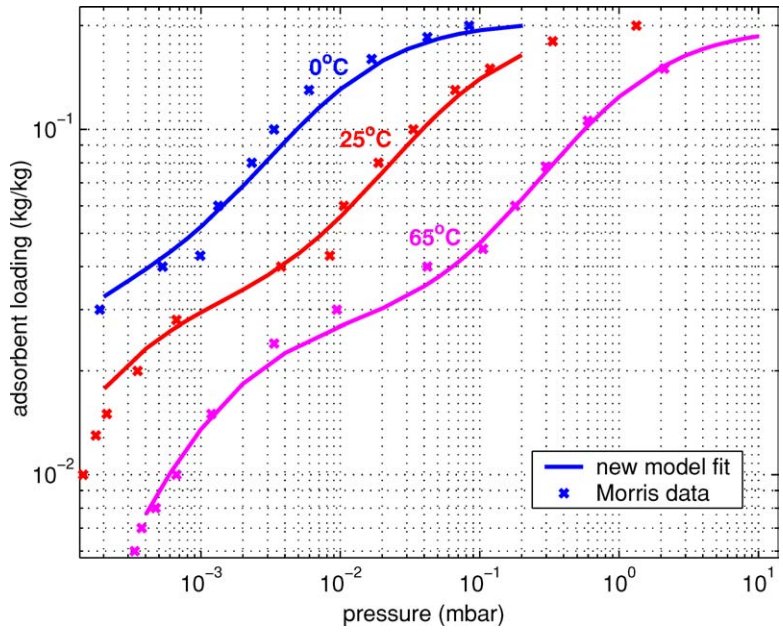

Figure 10. Literature data (Morris, 1968) of water vapor adsorption equilibria on Zeolite 4A at three different temperatures (symbols) in comparison to a model fit with the new approach (Eq. (1)) based on our measurements.

Table 3. Properties of adsorbent and other experimental information.

Column	Jacketed stainless steel				
Internal diameter D	0.01 m				
Length	0.797 m				
Adsorbent	Zeolite 4A				
Bed density ϱ_{sch}	736.5 kg/m^3				
Mass	0.0461 kg				
Mean pore radius	1086 Å				
Particle size d_p	0.001 m				
Specific surface area	21.9 m^2/g				
Gas void fraction ε	0.63				
Bed void fraction ε_b	0.4				
Specific heat capacity c_A	920 J/kg K				
Adsorbate j	Water				
Molar heat capacity c^0_{pj}	33.78 J/mol K				
Viscosity η_j	$1 \cdot 10^{-5}$ Pas				
Molecular weight M_j	0.01802 kg/mol				
Isosteric heat ΔH^{st}_j	54961 J/mol				
Carrier k	Synthetic air				
Molar heat capacity c^0_{pk}	29.19 J/mol K				
Viscosity η_k	$2 \cdot 10^{-5}$ Pas				
Molecular weight M_k	0.02896 kg/mol				
Experimental range	A	B	C	D	
Molar fraction of water $y_{j,f}$	4594	4410	4603	4531	ppm
Volumetric feed rate	1.84	1.998	2.00	1.98	Nl/min
Pressure p	5.0	2.0	2.0	2.0	bar
Wall temperature T_W	30	30	50	80	°C

3.2.2. Modeling. To derive information about the heat- and mass-transfer, the profiles of the breakthrough experiments are matched with computer simulations. The underlying mathematical model for temperature $T(z,t)$, pressure $p(z,t)$ and water mole fraction $y_j(z,t)$ in space z and time t is stated below.

Assuming the ideal gas law, the overall mass balance for the gas phase is given by

$$\frac{\varepsilon}{\mathbf{R}T}\left(\frac{\partial p}{\partial t} - \frac{p}{T}\frac{\partial T}{\partial t}\right) + \varrho_{\text{sch}}\frac{\partial q}{\partial t} = -\frac{1}{A}\frac{\partial \dot{n}}{\partial z}. \quad (4)$$

The component mass balance for water in the gaseous phase is

$$\frac{\varepsilon}{\mathbf{R}T}\left(y_j\frac{\partial p}{\partial t} - \frac{y_j p}{T}\frac{\partial T}{\partial t} + p\frac{\partial y_j}{\partial t}\right) + \varrho_{\text{sch}}\frac{\partial q_j}{\partial t} = -\frac{1}{A}\frac{\partial y_j \dot{n}}{\partial z}. \quad (5)$$

In addition, a quasi-homogeneous energy balance

$$\left(\varrho_{\text{sch}}c_A + \varepsilon\frac{p}{\mathbf{R}T}c^0_p + \varrho_{\text{sch}}c^0_{pj}q_j\right)\frac{\partial T}{\partial t} - \varepsilon\frac{\partial p}{\partial t} - \varrho_{\text{sch}}\Delta H^{st}_j\frac{\partial q_j}{\partial t} = \frac{4\alpha}{D}(T_w - T) - \frac{c^0_p}{A}\dot{n}\frac{\partial T}{\partial z} \quad (6)$$

is used. For the heat-transfer to the wall with constant temperature T_w, we use a constant overall heat transfer coefficient α. The molar flow $\dot{n}(z,t)$ is described by the stationary Ergun equation.

$$\begin{aligned} 0 &= \frac{\partial p}{\partial z} + f_1\dot{n} + f_2\dot{n}^2 \\ f_1 &= 150\eta\frac{\mathbf{R}T}{p}\frac{(1-\varepsilon)^2}{\varepsilon^3 d_p^2 A} \\ f_2 &= 1.75M\frac{\mathbf{R}T}{p}\frac{1-\varepsilon}{\varepsilon^3 d_p A^2} \end{aligned} \quad (7)$$

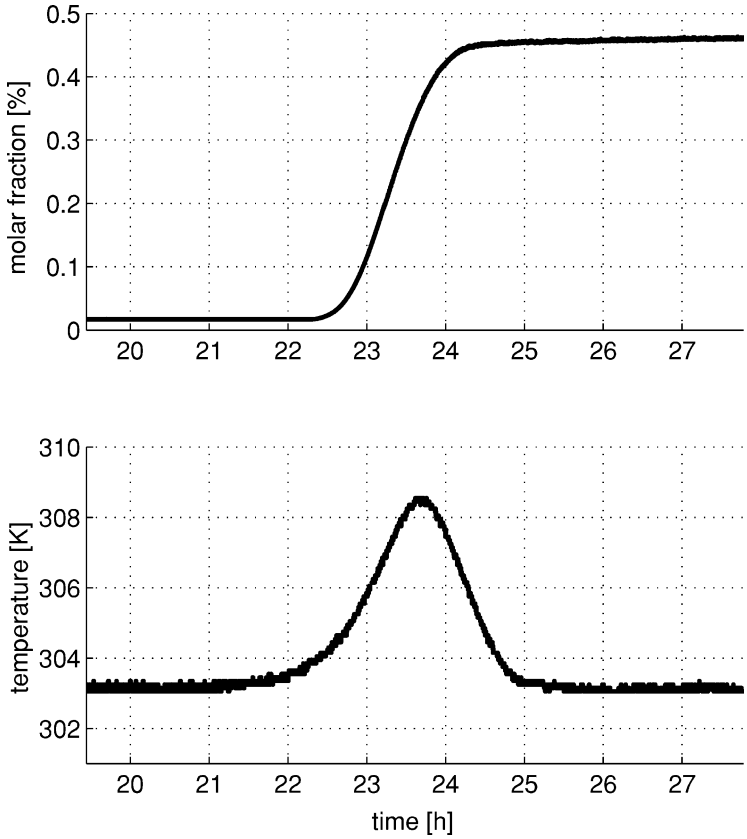

Figure 11. Breakthrough curves for case A: molar fraction of water and temperature.

For the mass balance of the adsorbed amount of water $q_j(z,t)$ a linear driving force (LDF) rate model has been assumed.[3]

$$\frac{\partial q_j}{\partial t} = K^{\mathrm{LDF}}(q_j^* - q_j) \tag{8}$$

The equilibrium loading $q_j^* = q_j^*(p, y_j, T)$ is calculated with the adsorption isotherm introduced in Eq. (1). The LDF model is a widely and successfully used lumped-parameter model for particle diffusion and adsorption (Sircar and Hufton, 2000). In the next section we will elaborate on the LDF coefficient K^{LDF}.

The periphery of the adsorber is modeled with an algebraic momentum balance for the valves (VDI/VDE norm 2173). The inital and boundary conditions corresponding to the partial differential equation system depend on the operating conditions and are not discussed in detail. After discretizing the spatial coordinate with finite volumes, a system of differential and algebraic equations (DAE) is obtained. It can be solved with efficient solvers like LIMEX (Deuflhard et al., 1987) or DASSL (Brenan et al., 1989). Since we use an upwind scheme on a staggered grid it is of great importance to chose the numbers of finite volumes such that the resulting numerical diffusion equals the theoretically expected physical dispersion. If so, the numerical solution of the hyberbolic PDAE above equals the solution of the corresponding parabolic PDAE with a dispersion term (Sokolichin, 2002).

3.2.3. Parameter Estimation. The mass-transfer coeffient K^{LDF} and the heat-transfer coeffient α are the two remaining unknowns which are used as adjustable parameters in fitting the simulated breakthrough profiles to the experiments. In agreement with the results reported by Malek and Farooq, the temperature breakthrough curve is moderately sensitive on the mass-transfer coefficient whereas the heat-transfer coefficient has no noticeable effect on the concentration profiles[4]. Hence, it is recommendable to first fit the concentration profile for K^{LDF} with a proper estimate

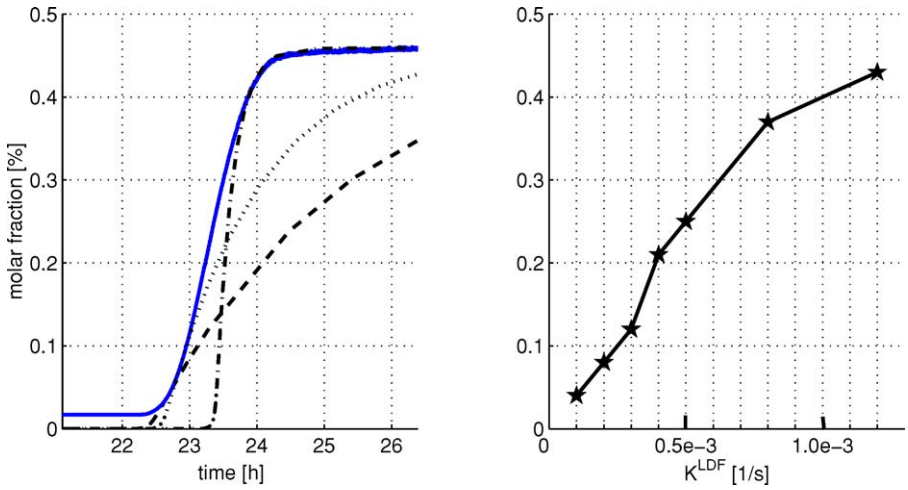

Figure 12. Left: Breakthrough curve of molar fraction of water for case A—experimental result (solid line) and simulations for different values of K^{LDF} (dashed, dotted, dot-dashed lines) and $\alpha = 50$ W/(m^{2}K). Right: values of K^{LDF} needed to match the slope of the experimental profile at the indicated molar fraction.

for α, and then fit the temperature profile for α if necessary.

Figure 12 (left) compares the experimental result for the breakthrough of the molar fraction of water (case A, Fig. 11) with simulations for different values of constant K^{LDF} ($\alpha = 50$ W/(m^{2}K)). It is important to note that the simulation results are shifted in time such that the simulated and measured profiles are tangent to each other at a certain water molar fraction y_j. The values of K^{LDF} needed to match the slope of the experimental profile at this particular molar fraction are shown in Fig. 12 (right). Now one can see that it is only possible to match the slope at a specific molar fraction but not the whole curve. Hence we must conclude that the mass-transfer coefficient K^{LDF} strongly depends on the concentration (Fig. 12, right) and thus can not be considered constant.

Ever since Glueckauf (1955) proposed the first and the most widely used approximation for modeling adsorption and diffusion in adsorbent particles (LDF model), numerous models have been developed which describe the overall rate of adsorption. Besides its simplicity, the success of this approach is due to its physical consistency (Hartzog and Sircar, 1995; Gemmingen, 1993; Raghavan et al., 1986; Chihara and Suzuki, 1983) and its numerical advantage compared to detailed pore models (Sircar and Hufton, 2000). However, depending on the process and the adsorptive system the attention has to be directed on required modifications of the classical approach. Such modifications can be necessary in order to take into account the influence of the heat of adsorption (Mendes et al., 1994; Sircar, 1983), of the dominating transport resistance in the pellet (Carta, 1993; Mendes et al., 1995, 1996; Taqvi and LeVan, 1996; Rodrigues and Dias 1998; Hufton and Sircar, 2000; Sircar and Hufton, 2000; Rouse and Brandini, 2001; Delgado and Rodrigues 2002), of the specific type of adsorption isotherm (Mendes et al., 1994; Zhang and Ritter, 1997; Gadre and Ritter, 2002), of the boundary conditions (Alpay and Scott, 1992; Buzanowski and Yang, 1991; Carta, 1993; Nakao and Suzuki, 1983) or the operating conditions (Raghavan et al., 1986).

To formulate a proper LDF approach for the considered water-Zeolite system, we first put the focus back on the work of Malek and Farooq. The individual mass-transer resistances for a biporous, spherical adsorbent are related to the K^{LDF} coefficient of Eq. (8) by the following equation:

$$\frac{1}{K^{\mathrm{LDF}}} = \frac{R_p}{3K_f}\frac{q_j^* \varrho_p}{c_j} + \frac{R_p^2}{15\,\varepsilon_p D_{\mathrm{eff}}}\frac{q_j^* \varrho_p}{c_j} + \frac{R_c^2}{15 D_c}. \quad (9)$$

For negligible mass-transfer resistance in the film and in the micropores this reduces to

$$\frac{1}{K^{\mathrm{LDF}}} = \frac{R_p^2}{15\varepsilon_p D_{\mathrm{eff}}}\frac{q_j^* \varrho_p}{c_j}. \quad (10)$$

Substituting the gas void fraction in the pellet ε_p with the overall gas void fraction ε, the particle density ϱ_p

with the bed density ϱ_{sch}

$$\varepsilon_p = \frac{\varepsilon - \varepsilon_B}{1 - \varepsilon_B}, \quad \varrho_p = \frac{\varrho_{\text{sch}}}{1 - \varepsilon_B}, \tag{11}$$

and applying the ideal gas law, Eq. (10) becomes:

$$\frac{1}{K^{\text{LDF}}} = \frac{R_p^2 \varrho_{\text{sch}} \mathbf{R} T}{15(\varepsilon - \varepsilon_B) D_{\text{eff}}} \frac{q_j^*}{p_j}. \tag{12}$$

Hereby, R_p is the pellet radius, p_j is the partial pressure of water and q_j^* is the corresponding equilibrium loading at the temperature T. The effective diffusivity D_{eff} is related to molecular (D_{mol}), Knudsen (D_k) and surface diffusion (D_s) as follows:

$$\frac{1}{D_{\text{eff}}} = \frac{\tau_p}{D_{\text{mol}}} + \frac{1}{\frac{D_k}{\tau_p} + \frac{1-\varepsilon_p}{\varepsilon_p} \frac{q_j^* \varrho_p}{c_j} \frac{D_s}{\tau_s}} \tag{13}$$

Now it is obvious to see that K^{LDF} depends on concentration c_j or partial pressure p_j through D_{eff} and the ratio $q_j^*(p_j, T)/p_j$ which is specified in the equilibrium relation (Eq. (1)). In the following we will substitute K^{LDF} in Eq. (8) by Eq. (12) and use D_{eff} as the fitting parameter which depends on concentration, pressure and temperature.

The influence of concentration can be studied in two different ways. Either D_{eff} is calculated from the K^{LDF}-values of Fig. 12, right, via Eq. (12) or D_{eff} is used directly as the optimization parameter to fit the breakthrough curves. Both procedures lead for case A to almost constant D_{eff}-values of about 6.510^{-7} m^2/s (Fig. 13). Hence, we can conclude that the dependency of the mass-transfer on concentration originates mainly from the adsorption equilibrium. This means that surface diffusion plays a minor role for the mass-transfer since it strongly depends on concentration, as shown in Eq. (13).

Figure 14 compares the experimental result for the breakthrough of the molar fraction of water and temperature (as shown in Fig. 11) with simulations for $D_{\text{eff}} = 6.8310^{-7}\text{m}^2/\text{s}$ and $\alpha = 50\,\text{W}/(\text{m}^2\text{K})$ and confirms the success of the procedure used.

To study the impact of temperature and pressure on the effective diffusivities, simulation profiles have been fitted to experimental data for the four cases A, B, C, D (Table 3). The results are shown in Fig. 15, (left). As before, the effective diffusivities do not depend noticeably on the molar fraction but they strongly depend on both pressure and temperature. Figure 15, (right), depicts this context in a logarithmic scale. If we assume a linear dependency on both states in the log-scale and connect the mean values of D_{eff} for each case, the resulting slope is close to -1 for the pressure and close to 1.75 for the temperature. To interpret this observation, let us first take a look at the

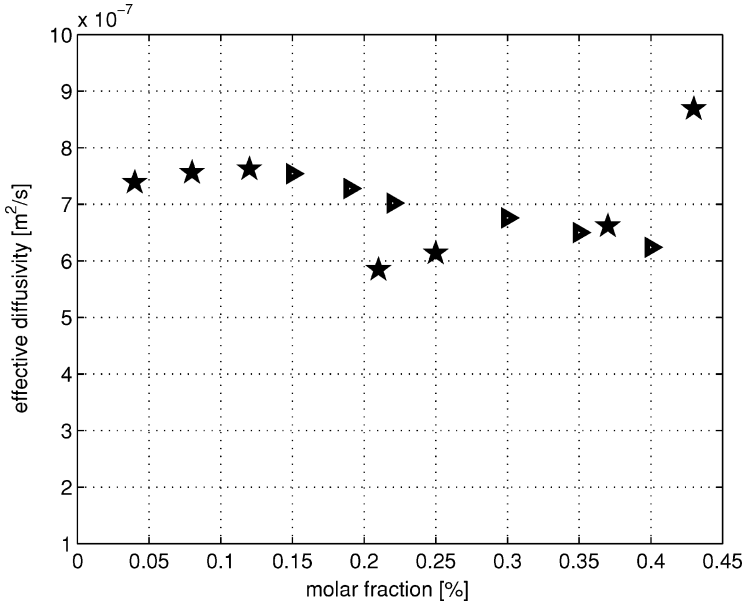

Figure 13. Effective diffusivity D_{eff} for case A calculated from K^{LDF} values of Fig. 12 (right) with Eq. (12) (stars) or from a direct fit to the slope of the breakthrough curve (triangles).

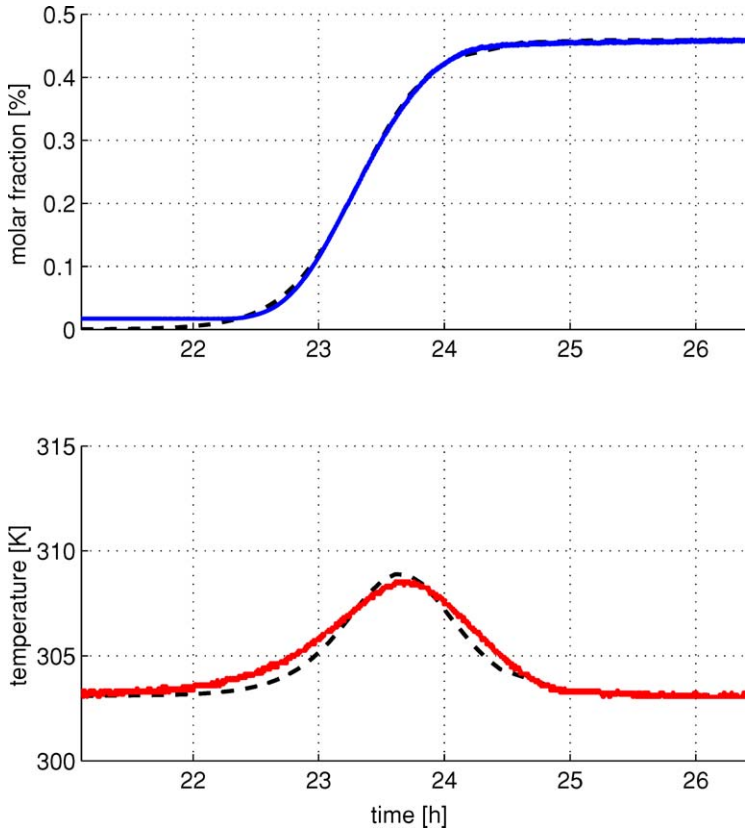

Figure 14. Breakthrough curves of molar fraction of water (top) and temperature (bottom) for case A—experimental results (solid lines) and simulation (dashed lines) for $D_{\text{eff}} = 6.83\,10^{-7}$ m^2/s and $\alpha = 50$ W/(m^{2}K).

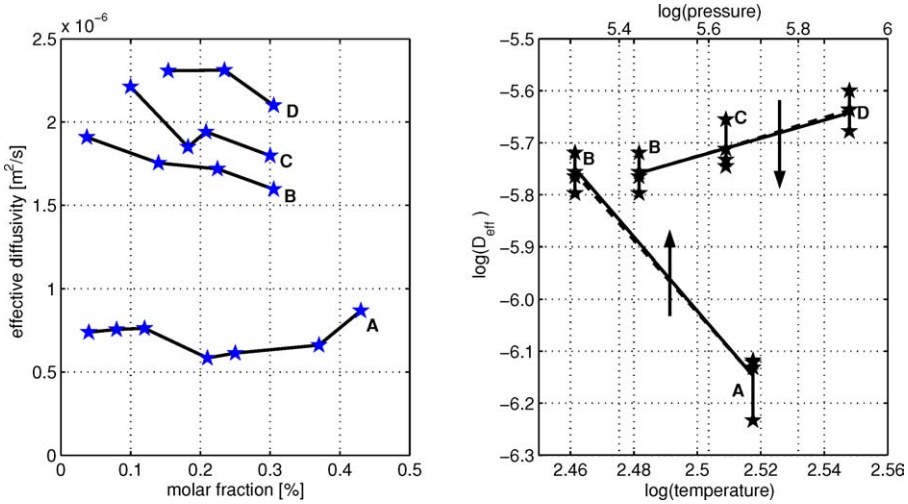

Figure 15. Left: Effective diffusivities over molar fraction needed to match the slope of the experimental profile for case A–D. Right: Effective mean diffusivities as a function of temperature and pressure in a log-scale. Dashed lines show the measured dependencies, solid lines indicate the theoretical dependencies assuming molecular diffusion only (Eq. (14)).

molecular diffusion coefficient D_{mol} used in Eq. (13). A well established correlation of Fuller, Schettler and Giddings (VDI-Wärmeatlas, 1988) for binary mixtures is:

$$D_{\mathrm{mol}} = \frac{10^{-3} T^{1.75} \left(\frac{M_1+M_2}{M_1 M_2}\right)^{0.5} 1.013}{p\left[\left(\sum \nu_1\right)^{1/3} + \left(\sum \nu_2\right)^{1/3}\right]^2}. \qquad (14)$$

Besides of the molecular weights M_i and the diffusion volumes ν_i, D_{mol} depends on temperature and pressure leading to:

$$\log(D_{\mathrm{mol}}) = f(M_i, \nu_i) + 1.75 \log(T) - \log(p). \qquad (15)$$

If we compare Eq. (15) with the results shown in Fig. 15, (right), it follows that the mass-transfer into the pellet must be primarily governed by molecular diffusion since the slopes in the log-scale are almost the same. Since we have now established and interpreted the temperature-, pressure- and (the negligible) concentration-dependency of D_{eff}, we may specify a reference effective diffusivity D^0_{eff}:

$$D^0_{\mathrm{eff}} = D_{\mathrm{eff}} \frac{p}{T^{1.75}}. \qquad (16)$$

Thus, we can write Eq. (12) in the form:

$$K^{\mathrm{LDF}}(y_j, p, T) = D^0_{\mathrm{eff}} \frac{15(\varepsilon - \varepsilon_B)}{R_p^2 \varrho_{\mathrm{sch}} \mathbf{R}} \frac{T^{0.75}}{p} \frac{p_j}{q_j^*}. \qquad (17)$$

Combining the invariant terms to one kinetic coefficient Θ and with $p_j = y_j p$ we finally obtain:

$$K^{\mathrm{LDF}}(y_j, p, T) = \Theta \frac{y_j T^{0.75}}{q_j^*(y_j, T, p)}. \qquad (18)$$

For case A with $D_{\mathrm{eff}} = 6.8310^{-7}$ m^2/s the reference effective diffusivity is $D^0_{\mathrm{eff}} = 1.55 \cdot 10^{-5} \cdot \Theta$ becomes $3.45 \cdot 10^{-2}$ if SI units are used.

Combining Eqs. (8) and (18), the mass balance for the adsorbed amount of water becomes:

$$\frac{\partial q_j}{\partial t} = \Theta\, y_j T^{0.75} (1 - q_j/q_j^*). \qquad (19)$$

To evaluate the capability of Eq. (19) for describing the adsorption kinetics properly, Fig. 16 shows the simulation results in comparison with the experimental breakthrough profiles for case A, B, C and D. As a final result we can point out that the suggested approach (Eq. (19)) predicts the breakthrough curves properly. Hence, the above equation represents a very simple but sufficient

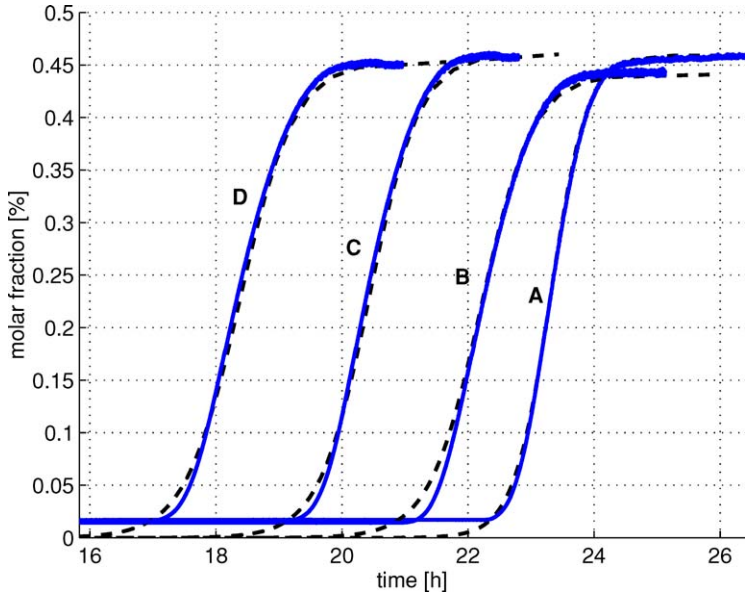

Figure 16. Breakthrough curves of molar fraction of water for case A, B, C and D (Table 3): experimental results (solid lines) and simulations (dashed lines) based on Eq. (18) with $\Theta = 0.0345$.

model for the kinetics of water vapor adsorption on Zeolite 4A. In the feasible range of operating conditions for air drying via pressure swing adsorption, it is thus possible to model adsorption kinetics based on only one constant parameter, Θ.

4. Concluding Remarks

In this paper we have examined the water vapor adsorption on Zeolite 4A. A volumetric high vacuum apparatus has been used to measure adsorption isotherms over a wide range of partial pressure. Several conventional isotherm models were fitted to the obtained data. Due to their lack of fit especially in the very low pressure range, a new type of isotherm model was presented. With five temperature dependent parameters it is possible to match all experiments sufficiently well. The characteristic shape of the isotherm is explained by two different adsorption sites of a completly dehydrated zeolite.

In order to evaluate adsorption kinetics, breakthrough experiments at different temperatures and bed pressures were performed. A mathematical model for the process based upon a linear driving force equation for the mass-transfer is provided. The linear driving force coefficient K^{LDF} is considered to change with concentration, pressure and temperature. The strong dependence on concentration could be described by the nonlinearity of the adsorption isotherm. Its temperature and pressure dependence proved to correspond to that of binary molecular diffusion. As a result, a well founded simple and accurate model for the kinetics of water vapor adsorption on Zeolite 4A as a function of pressure, temperature and molar fraction of water has been established. It contains only one kinetic coefficient, which in the treated region of operating conditions is a constant and can easily be determined from one breakthrough experiment. This surprisingly simple result is considered a consequence of the fact that for trace water adsorption from air the decisive pore transport mechanism is molecular diffusion of water in stagnant air.

Future work will be focused on applying the model presented in this work to a PSA system for air drying.

Nomenclature

A	Cross-section
c_j	Water concentration
b	Parameter of adsorption isotherm
c_p^0	Molar heat capacity
c_A	Specific heat capacity of pure adsorbent
d_p	Pellet diameter
D	Inner column diameter
D_c	Micropore diffusivity
D_{eff}	Effective diffusivity
D_{eff}^0	Reference effective diffusivity
D_k	Knudsen diffusivity
D_{mol}	Molecular diffusivity
D_s	Surface diffusivity
$f_{1/2}$	Coefficient of the Ergun equation
ΔH^{st}	Isosteric heat of adsorption
K^{LDF}	Linear driving force coefficient
K_f	Film mass transfer coefficient
M	Molecular weight
$\dot{n}$	Molar flow
p	Pressure
p_j	Partial pressure
$\mathbf{R}$	Universal gas constant (=8.3143 J/molK)
R_c	Microparticle radius
R_p	Pellet radius
t	Time
T	Temperature
T_0	Reference temperature (=273.25 K)
T_W	Wall temperature
q_j	Adsorbent loading in mol_j/kg
q_j^*	Saturation loading in mol_j/kg
X_j	Adsorbent loading in kg/kg
y_j	Molar fraction of water in air
z	Space dimension

Greek Letters:

α	Heat transfer coefficient
η	Dynamic viscosity
ε	Gas void fraction
ε_b	Bed void fraction
ε_p	Particle void fraction
ϱ_p	Particle density
ϱ_{sch}	Bed density
Φ	Relative humidity
ν	Diffusion volume
τ_p	Particle tortuosity
τ_s	Surface tortuosity
Θ	Kinetic coefficient

Acknowledgments

The authors are grateful to the Deutsche Forschungsgemeinschaft for their financial support.

Notes

1. Both reproducible experiments and calculations with a 3D-CAD tool yield identical results for the volumes.
2. Although water vapor at low pressures can be considered ideal, we use a Redlich-Kwong-Soave real gas approach.
3. It has been shown earlier (Taqvi and Le Van, 1996; Scholl et al., 1993) that for a trace component system the role of intraparticle convection can be neglected.
4. A variation of α from 10 to 200 W/(m^2K) in the above model did not affect the breakthrough curve visibly.

References

Alpay, E. and D.M. Scott, "The Linear Driving Force Model for Fast-Cycle Adsorption and Desorption in a Spherical Particle," *Chem. Eng. Sci.*, **47**, 499–502 (1992).

Breck, D.W., W.G. Eversole, R.M. Milton, T.B. Reed, and T.L. Thomas, Crystalline Zeolites. I. The Properties of a New Synthetic Zeolite, Type A, *J. Am. Chem. Soc.*, **78**, 5963–5971 (1956).

Brenan, K.E., S.L. Campbell, and L.R. Petzold, *Numerical Solution of Initial-Value Problems in Differential-Algebraic Equations*, North-Holland, 1989.

Brunauer, S., L.S. Deming, W.E. Deming, and E.J. Teller, *J. Am. Chem. Soc.*, **62**, 1723 (1940).

Buzanowski, M.A., and R.T. Yang, "Approximations for Intraparticle Diffusion Rates in Cyclic Adsorption and Desorption," *Chem. Eng. Sci.*, **46**, 2589–2598 (1991).

Carta, G., "The Linear Driving Force Approximation for Cyclic Mass Transfer in Spherical Particles," *Chem. Eng. Sci.*, **48**, 622–625 (1993).

Chihara, K. and M. Suzuki, "Simulation of Nonlinear Pressure Swing Adsorption," *J. Chem. Eng. Japan*, **16**, 53–61 (1983).

Delgado, J.A. and A.E. Rodrigues, "A Stefan-Maxwell Model of Single Pore Pressurization for Langmuir Adsorption of Gas Mixtures," *Adsorption*, **7**, 171–187 (2001).

Deuflhard, P., E. Hairer, and J. Zugck, "One Step and Extrapolation Methods for Differential Algebraic Systems," *Numer. Math.*, **51**, 501–516 (1987).

Gadre, S.A. and J.A. Ritter, "New Analytical Solution for Nonlinear Adsorption and Diffusion in a Single Particle," *Chem. Eng. Sci.*, **57**, 1197–1204 (2002).

Gemmingen, U. von, "Pressure Swing Adsorption Process—Design and Simulations," in *Proceedings of the IVth Int. Conf. on Fundamentals of Adsorption*, M. Suzuki (Ed.), pp. 703–712, Kyoto, Kodansha, Japan, 1993.

Glueckauf, E., "Theory of Chromatography," *Trans. Faraday Soc.*, **51**, 1540–1551 (1955).

Hartzog, D.G. and S. Sircar, "Sensitivity of PSA Process Performance to Input Variables," *Adsorption*, **1**, 133 (1995).

Hufton, J.R. and S. Sircar, "Intraparticle Adsorbate Concentration Profile for Linear Driving Force Model," *AIChE Journal*, **3**, 659–660 (2000).

Malek, A. and S. Farooq, "Kinetics of Hydrocarbon Adsorption on Activated Carbon and Silica Gel," *AIChE Journal*, **43**, 761–776 (1997).

Mendes, A.M.M., C.A.V. Costa, and A.E. Rodrigues, "Linear Driving Force Approximations for Diffusion in Spherical Adsorbents with Binary Non-Linear Adsorption," *Gas Sep. Pur.*, **8**, 229–236 (1994).

Mendes, A.M.M., C.A.V. Costa, and A.E. Rodrigues, "Linear Driving Force Approximation for Isothermal Non-Isobaric Diffusion/Convection with Binary Langmuir Adsorption," *Gas Sep. Pur.*, 259–270 (1995).

Mendes, A.M.M., C.A.V. Costa, and A.E. Rodrigues, "Extension of the Linear Driving Force—Dusty Gas Model Approximation to Include Surface or Micropore Diffusion," *Gas Sep. Pur.*, **10**, 141–148 (1996).

Morris, B., "Heats of Sorption in the Crystalline Linde-A Zeolite-Water Vapor System," *J. Colloid Interface Sci.*, **28**, 149–155 (1968).

Münstermann, U., A. Mersmann, and J. Schadl, "Non-Isothermal Multicomponent Adsorption and Desorption of CO_2 and H_2O on Molecular Sieve," *Ger. Chem. Eng.*, **6**, 1–8 (1983).

Nakao, S. and M. Suzuki, "Mass Transfer Coefficient in Cyclic Adsorption and Desorption," *J. Chem. Eng. Japan*, **2**, 114–119 (1983).

Raghavan, N.S., M.M. Hassan, and D.M. Ruthven, "Numerical Simulation of a PSA System Using a Pore Diffusion Model," *Chem. Eng. Sci.*, **11**, 2787–2793 (1986).

Rouse, A.J. and S. Brandini, "Efficient Modelling of Fast Cycle Adsorption for the Seperation of CO_2," University College London, 2001.

Rodrigues, A.E. and M.M. Dias, "Linear Driving Force Approximation in Cyclic Adsorption Processes: Simple Results from System Dynamics Based on Frequency Response Analysis," *Chem. Eng. Proc.*, **37**, 489–502 (1998).

Ruthven, D.M., *Pressure Swing Adsorption*, John Wiley & Sons, 1984.

Scholl, S., H. Kajszika, and A. Mersmann, "Adsorption and Desorption Kinetics in Activated Carbon," *Gas Sep. Purif.*, **7**, 207–212 (1993).

Sircar, S., "Linear-Driving-Force Model for Non-Isothermal Gas Adsorption Kinetics," *J. Chem. Soc. Faraday Trans. 1*, **79**, 785–796 (1983).

Sircar, S. and J.R. Hufton, "Why does the Linear Driving Force Model for Adsorption Kinetics Work," *Adsorption*, **6** 137–147 (2000).

Skarstrom, C.W., "Heatless Fractionation of Gases Over Solid Adsorbents," *Recent Developments in Separation Science*, **2**, 95–106 (1972).

Sokolichin, A., *Mathematische Modellbildung und numerische Simulation von Gas-Flüssigkeits Blasenströmungen*, Monograph, Universität Stuttgart, 2002.

Taqvi, S.M. and M.D. LeVan, "Role of Convection and Diffusion in a Single Pore with Adsorptive Walls," *Adsorption*, **2**, 299–309 (1996).

VDI-Wärmeatlas, VDI-Verlag GmbH Düsseldorf, 1988.

Zhang, R. and A. Ritter, "New Approximate Model for Nonlinear Adsorption and Diffusion in a Single Particle," *Chem. Eng. Sci.*, **52**, 3161–3172 (1997).

Zhdanov, S.P., S.S. Khvoshchev, and N.N. Feoktistova, *Sinteticheski Tseolity*, Khimiya, 1981.